ICCAUA Proceedings Journal
Proceedings of the international conference of contemporary affairs in architecture and urbanism-ICCAUA
Volume 9 (December 2026), 2610484

Journal homepage: https://journal.iccaua.com/

DOI: https://doi.org/10.38027/ICCAUA2026EN0484

Full-Field Deformation Measurement and Debonding Analysis in Masonry-Infilled RC Frames Under Lateral Loading

* [1] **Ismail Layadi**
[1] Applied Civil Engineering Laboratory (LGCA), Civil Engineering Department, Echahid Cheikh Larbi Tebessi University, Tebessa, Algeria
[1] E-mail: ismail.layadi@univ-tebessa.dz
[1] ORCID: https://orcid.org/0000-0002-4808-953X

Received: 25.04.2026
Revised: 27.06.2026
Accepted: 01.07.2026
Available online: 10.07.2026

This article has been selected and peer-reviewed for publication in this journal as part of the 9th International Conference of Contemporary Affairs in Architecture and Urbanism, held on 7–8 May 2026 in Istanbul, Türkiye.

Abstract

This study investigates the in-plane lateral behavior of reinforced concrete (RC) frames with masonry infill walls, addressing their critical yet frequently overlooked role in seismic design. Four half-scale specimens, two bare frames and two with double-leaf masonry infills, were subjected to lateral cyclic and monotonic loading. High-resolution Digital Image Correlation (DIC) was utilized to precisely monitor strain, displacement, and interface slip. Results show that infills significantly increase maximum lateral strength (2.6-2.7 times) and initial stiffness (4.4-5.3 times) compared to bare frames, but reduce displacement ductility and exacerbate stiffness degradation. Crucially, DIC revealed that initial gaps from construction sequencing trigger early interface debonding at roughly 75% of peak load, initiating a diagonal strut mechanism that imposes severe shear demands on beam-column joints. This research uniquely links local construction practice to structural resilience and validates DIC as an advanced diagnostic tool for mapping complex frame-wall interactions.
Keywords: Masonry infilled frames; Digital Image Correlation; Wall-frame interaction; Debonding Analysis, In-plane behavior.

1. Introduction

Masonry infill walls are ubiquitous in reinforced concrete (RC) frame structures throughout earthquake-prone regions, particularly in North Africa, the Mediterranean basin and the Middle East. Historically treated as non-structural partitions, these walls have repeatedly proven their structural significance during major seismic events. The 2003 Boumerdes earthquake in Algeria, for instance, demonstrated that the interaction between masonry infills and RC frames can dramatically alter the lateral stiffness, strength and failure mechanism of a building, either beneficially or detrimentally depending on configuration (Ghorbani et al., 2014). Recent comprehensive reviews have synthesized decades of experimental and analytical research on the seismic performance of masonry-infilled RC frames, highlighting persistent challenges in design code treatment and the need for integrated frame-infill design approaches (Pokharel et al., 2024). Despite this, many design codes still treat infill walls as architectural elements, neglecting their contribution to or interference with lateral load resistance.

The structural role of masonry infill walls has been extensively debated in the literature. When subjected to in-plane lateral loading, infills transform an otherwise flexible RC frame into a stiffer system by activating a diagonal compression strut mechanism (Mehrabi et al., 1996). This mechanism substantially increases lateral stiffness and peak strength but simultaneously reduces ductility and concentrates damage at beam-column joints and infill corners (Demirel et al., 2023). The degree to which these effects manifest depends critically on the quality of the frame-infill interface, the construction sequence, and the material properties of both the frame and the masonry panel.

A central but underexplored issue is the effect of construction sequencing on frame-infill interaction. In Algeria, as in much of North Africa, the standard practice is to erect the RC frame first and subsequently construct the masonry infill within the completed bays. This sequence inevitably produces small gaps and imperfect mortar joints at the frame-infill interface, which weaken the bond and alter the debonding behaviour under lateral loading compared to systems where masonry is integrated monolithically with the frame, such as confined masonry (Ghorbani et al., 2014).

Experimental research on infilled frames has advanced considerably, with tests ranging from component-level wall specimens to full-scale multi-storey buildings under pseudodynamic excitation (Kallioras et al., 2023). Single-bay experimental configurations have also proven valuable for isolating frame-infill interaction effects characterizing failure modes under controlled laboratory conditions (Grubišić et al., 2023). However, measurement techniques have largely relied on traditional contact sensors, which provide only local, point-wise displacement and force data. These methods are inherently unable to capture the rich spatial evolution of damage, the development of diagonal crack patterns, or the progressive debonding along the frame-infill interface.

Digital Image Correlation (DIC) has emerged as a powerful full-field, non-contact measurement technique capable of resolving surface displacements and strains at high resolution across the entire face of a specimen. By comparing successive digital photographs taken during loading to a reference image, DIC reconstructs displacement and strain fields without physical contact, making it ideal for capturing subtle crack initiation, strain localisation and interface slip (Sciuti et al., 2025; Bhat et al., 2024). Lu et al. 2024 recently demonstrated the effectiveness of DIC in mapping hysteresis performance and damage evolution in masonry-infilled frames under cyclic loading, validating its capability to resolve complex frame-infill interaction mechanisms that conventional instrumentation cannot capture. Despite its potential, systematic application of DIC to masonry-infilled RC frames under lateral loading remains limited in the existing literature.

Despite extensive research on infilled frames, two gaps remain. First, the systematic application of full-field DIC to map the progressive debonding and relative slip at the frame–infill interface, as opposed to point-wise contact measurement, is still scarce. Second, the specific influence of the construction sequence prevalent across North Africa and much of the developing world, in which the masonry panel is built after the surrounding frame, has rarely been quantified experimentally despite its direct effect on the as-built interface and on seismic vulnerability.

This paper addresses both gaps. It presents an experimental investigation of four half-scale RC frames, two bare and two with double-leaf masonry infill walls representative of current Algerian construction practice, subjected to monotonic and cyclic lateral loading, with high-resolution DIC applied throughout to map full-field strain and displacement fields. The specific objectives are: (i) to characterise and compare the lateral strength, stiffness and ductility of bare and infilled frames; (ii) to identify failure modes and crack-propagation sequences using DIC; (iii) to quantify stiffness degradation and energy dissipation under cyclic loading; and (iv) to analyse the progressive debonding and relative slip at the frame–infill interface in detail. The principal contribution of the study is twofold: methodologically, it demonstrates and validates DIC as a quantitative diagnostic tool capable of resolving interface kinematics that conventional instrumentation cannot capture; and substantively, it establishes a direct, measurable link between a widespread construction practice and the debonding mechanism that governs the seismic load path. These findings extend the existing literature, which has largely treated the frame-infill bond as idealized, and offer experimental evidence relevant to the calibration of contact-friction interface models, aligning with the conference's scope on contemporary affairs in architecture, urbanism and the resilience of the built environment.

2. Materials and Methods

This study followed a structured experimental methodology organised into four sequential phases, as summarised in the methodological framework of Figure 1. In Phase I (Design and Fabrication), four half-scale RC frame specimens, two bare and two masonry-infilled, were designed in accordance with Algerian regulations and constructed following local practice. In Phase II (Test Configuration), each specimen was instrumented and mounted on the reaction frame, with vertical pre-load and horizontal actuators, boundary restraints, and contact transducers installed. In Phase III (Full-Field Acquisition), a 2D Digital Image Correlation (DIC) system recorded the surface displacement and strain fields synchronously with the applied force and the conventional transducers throughout loading. Finally, in Phase IV (Post Processing and Analysis), the acquired images and signals were processed to extract force–displacement responses, crack and strain maps, stiffness and ductility indices, energy dissipation, and frame–infill interface kinematics. Each phase is detailed in the subsections below.

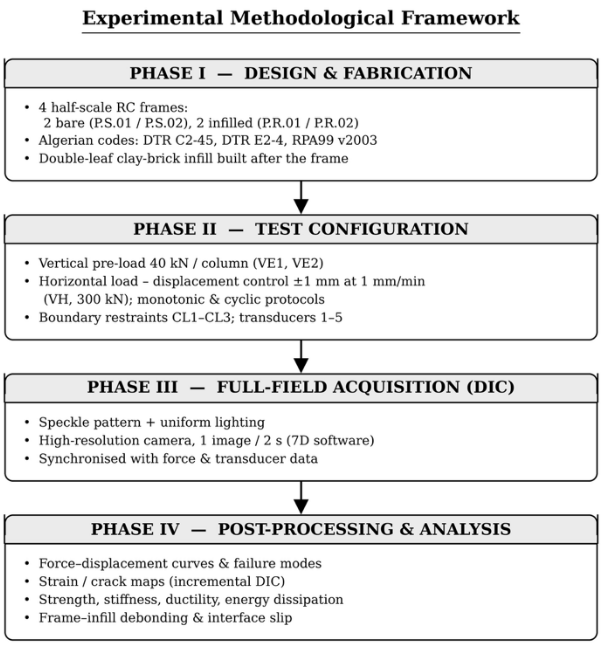

Figure 1. Methodological framework of the experimental programme, showing the four sequential phases from specimen design to full-field DIC analysis (Source: Authors).

2.1 Specimen Design and Construction

The experimental programme comprised four single-storey, single-bay RC frame specimens, designated P.S.01, P.S.02 (bare frames) and P.R.01, P.R.02 (masonry-infilled frames), as summarised in Table 1. The specimens were designed at half-scale relative to a typical Algerian residential frame with a storey height of 3.06 m and a bay span of 3.5-4.0 m. The scaled specimens have a clear height of 1.52 m and a span of 2.06 m. All design decisions were governed by Algerian construction regulations: DTR C2-45 (concrete design), DTR E2-4 (steel reinforcement) and the Algerian seismic code RPA99 version 2003.

Columns and beams have identical 250 x 250 mm square cross-sections, reinforced with four 12 mm high-bond longitudinal bars and 6 mm smooth stirrups. The foundation beam (longrine) has a 300 x 400 mm cross-section and was cast with protruding starter bars to ensure continuity of reinforcement at the column base, replicating in-situ frame-foundation conditions. Concrete and steel materials were sourced from local Algerian suppliers; cement was provided by the Tebessa cement factory (SCT). Duplicate specimens of each type were produced to verify experimental reproducibility.

Infill walls were constructed using 100 x 200 x 300 mm hollow clay bricks manufactured in Algeria (NF P13-301), arranged in a double-leaf configuration with a 50 mm central air gap, consistent with prevailing Algerian practice. Horizontal and vertical mortar joints are 10 mm thick. The masonry infill was constructed after the surrounding RC frame had hardened, following the construction sequence most common in Algeria and deliberately leaving a small gap between the panel perimeter and the frame. This gap, filled with a thin mortar layer of variable quality, governs the early-stage frame-infill interaction.

Table 1: Description of test specimens.

Reference	Frame Type	Loading Protocol
P.S.01	Bare frame	Monotonic
P.S.02	Bare frame	Cyclic (load/unload)
P.R.01	Infilled frame	Monotonic
P.R.02	Infilled frame	Cyclic (load/unload)

2.2 Test Setup and Loading Protocol

Testing was carried out at the LOCIE laboratory, Universite Savoie Mont Blanc, France, in collaboration with the LGCA laboratory, Universite de Tebessa, Algeria. Each specimen was mounted on a rigid testing frame and subjected to two stages of loading. First, a constant vertical pre-load of 40 kN per column was applied through two electric actuators (VE1, VE2; capacity 120 kN each) operating under force control with 10 kN increments, simulating the weight of an upper floor slab. This pre-load was maintained throughout the remainder of the test.

Second, a horizontal displacement was applied at the top of the frame through a hydraulic actuator (VH; capacity 300 kN) operating under displacement control. Displacement was applied in increments of +/-1 mm at a rate of 1 mm/min until failure. For monotonic tests (P.S.01, P.R.01), displacement was applied in a single direction. For cyclic specimens (P.S.02, P.R.02), each displacement increment was applied as a complete load-unload cycle before proceeding to the next amplitude. Boundary conditions were enforced by three restraint systems: lateral clamps (CL1) to prevent out-of-plane buckling; vertical tie-rods (CL2) to prevent uplift; and horizontal steel wedges (CL3) to prevent base sliding. Five displacement transducers (comparators 1-5) monitored lateral displacement, frame rocking, base sliding, out-of-plane displacement, and testing frame deformation, respectively.

2.3 Digital Image Correlation Setup

The full-field strain and displacement measurement system used 2D Digital Image Correlation implemented in the 7D software (Vacher et al., 1999). Prior to testing, a high-contrast speckle pattern (mouchetis) was applied by spray paint over the specimen face to create the random texture required for DIC tracking. Two powerful lamps were positioned to provide uniform illumination across the specimen surface throughout the test. A high-resolution digital camera continuously captured images of the specimen face at two-second intervals throughout loading, synchronised with the acquisition system recording actuator forces and transducer readings. Post-processing compared each deformed image to the reference (unloaded) image to compute displacement and maximum principal strain fields across the entire specimen face. For improved visualisation of crack evolution, an incremental analysis was performed: each image at loading stage N was compared with the image at stage N-1 rather than with the original reference.

3. Results

3.1 Failure Modes and Crack Patterns

Figure 2 illustrates the advantage of DIC over naked-eye observation: while only major cracks were visible to the naked eye, the DIC strain maps revealed fine crack networks at very early loading stages, providing a more complete and quantitatively detailed picture of damage progression.

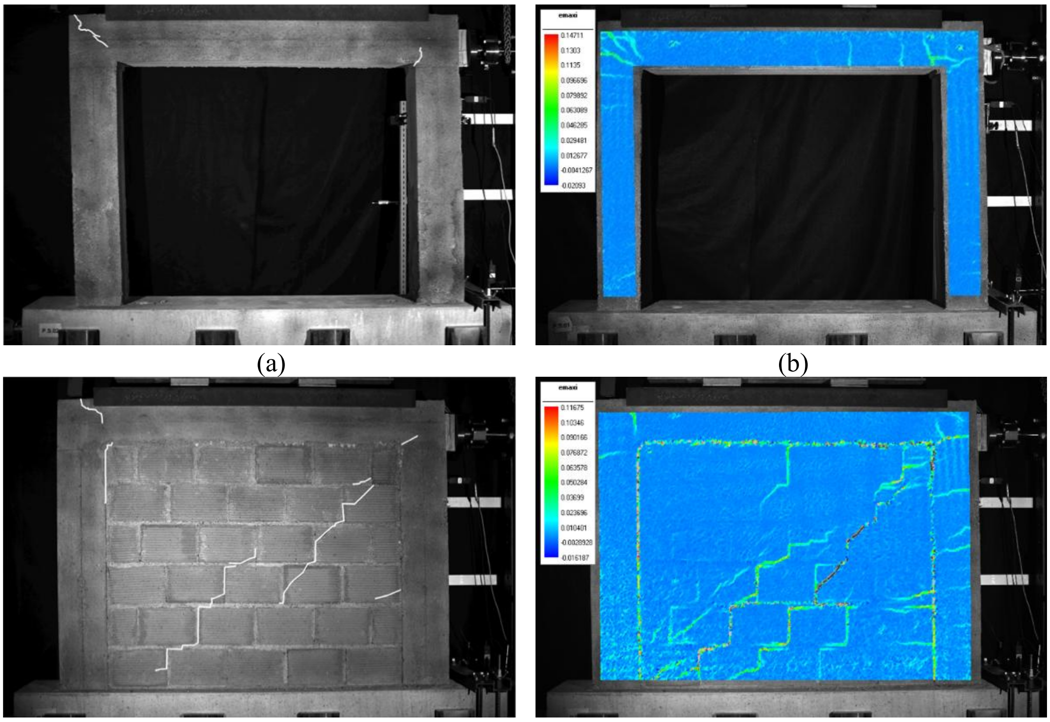

(a) (b) (c) (d)

Figure 2. Comparison of crack patterns: (a, c) visible to the naked eye; (b, d) mapped by DIC maximum principal strain fields, for bare frame P.S.01 and infilled frame P.R.01 respectively (Source: Authors).

Bare frames (P.S.01 and P.S.02): Both bare specimens exhibited nearly identical flexure-dominated behaviour. At loading point A, cracking initiated at the left beam-column joint (Figure 3). A vertical crack appeared in the beam at approximately one-third of the span from the loaded side. At point B, cracking extended to the right beam-column joint and widened on the left. Stiffness degradation became apparent as loading continued to the peak (point C: 76.1 kN at 24.3 mm for P.S.01; 76.4 kN at 15.9 mm for P.S.02). Post-peak (point D), deformation concentrated in the beam-column connection zones, leading to specimen failure by beam-column joint hinging. The two bare frames showed high ductility; post-peak resistance declined slowly even at displacements twice the peak displacement.

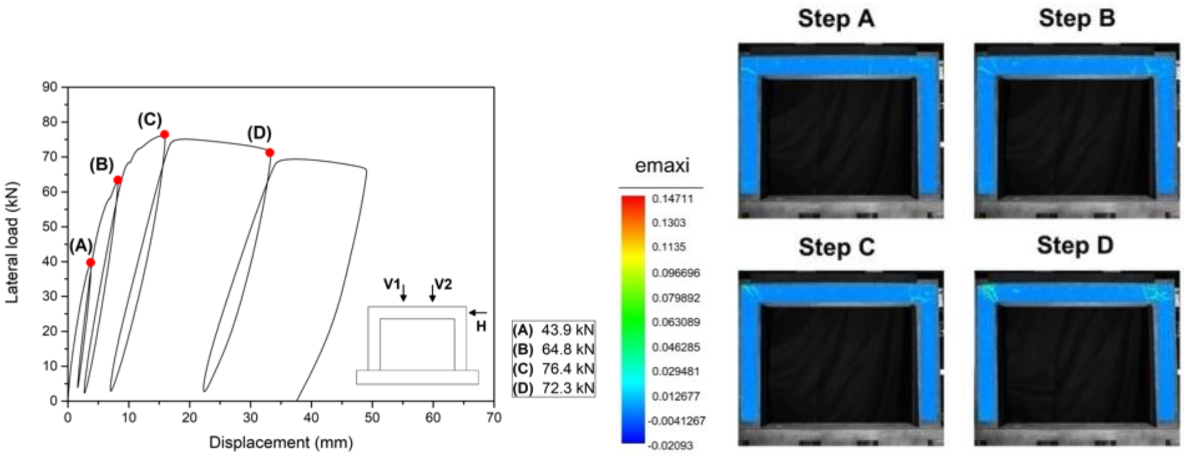

Figure 3. The DIC strain fields for specimen P.S.02.

Infilled frames (P.R.01 and P.R.02): Infilled specimens displayed a markedly different and more complex failure sequence. At the earliest loading stage (point A; 52.4 kN / 0.59 mm for P.R.01; 59.1 kN / 0.64 mm for P.R.02), DIC revealed the onset of frame-infill separation at the upper-left corner of the panel-frame contact, attributed to the imperfect mortar joint resulting from constructing the infill after the frame (Figure 4). This debonding progressively extended around the full perimeter by point B. Diagonal cracking initiated in the masonry panel at point B for P.R.01, starting in mortar joints at the panel centre and upper-right corner. For P.R.02, initial cracking was observed at the frame (shear cracks in beam-column joints and a flexural crack on the right column) before spreading into the panel. By loading point D, the classical staircase-pattern diagonal crack was fully formed in both infilled specimens: a single dominant diagonal for P.R.01 and two parallel diagonal cracks for P.R.02. Post-peak (point E-F), deformation concentrated near the upper-right corner, ultimately leading to localised brick crushing as illustrated in Figure 5.

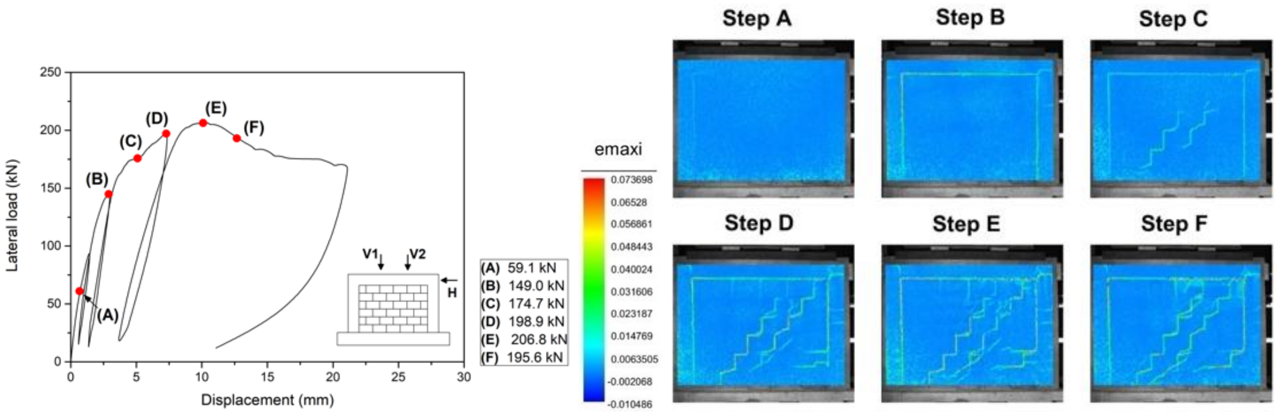

Figure 4. The DIC strain fields for specimen P.R.02.

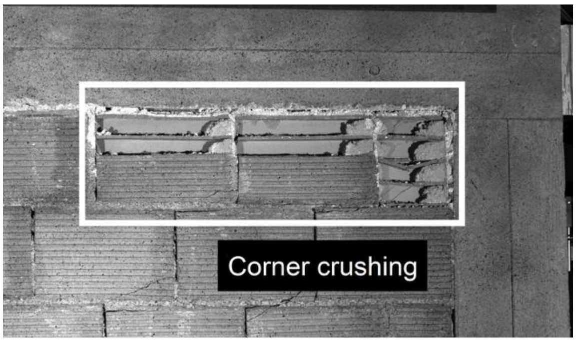

Figure 5. Crushing of brick elements at the upper-right corner of specimen P.R.02 at post-peak loading (Source: Authors).

3.2 Lateral Strength and Force-Displacement Response

Figure 6 presents the force-displacement curves for all four specimens. For monotonic tests, the full curve is shown; for cyclic specimens, the envelope curve connecting the peaks of successive cycles is plotted alongside for direct comparison with the monotonic response. The envelope curves closely match the monotonic curves for both frame types, confirming the repeatability of results and the material memory effect documented by Mehrabi et al. (1996). This equivalence also implies that the load/unload (push-over) cyclic protocol used here does not capture fatigue damage, which would require reversed-cycle (push-pull) loading.

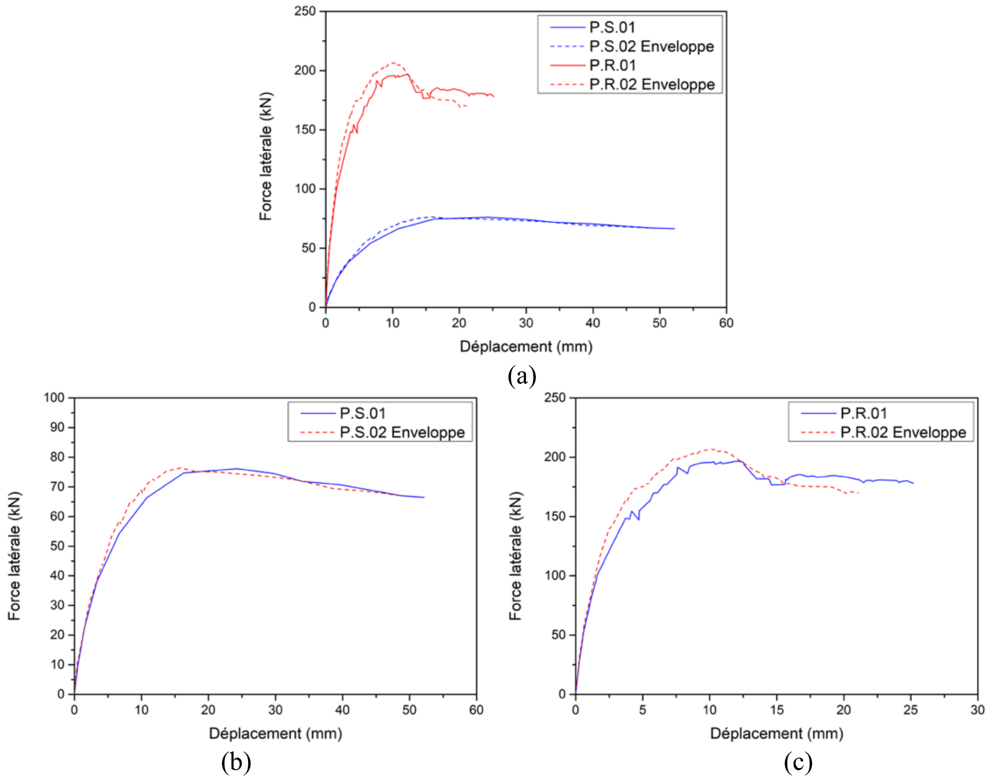

Figure 6. Force-displacement responses: (a) all specimens; (b) bare frames P.S.01 vs P.S.02 envelope; (c) infilled frames P.R.01 vs P.R.02 envelope (Source: Authors).

Table 2 summarises the peak lateral strength Fmax for all specimens. Bare frames reached 76.1 kN (P.S.01) and 76.4 kN (P.S.02), while infilled frames reached 196.7 kN (P.R.01) and 206.8 kN (P.R.02). Taking the bare frame capacity as unity, the infilled frames achieved lateral strength ratios of 2.6 and 2.7, respectively. These values are consistent with published ratios from comparable experimental programmes (Mehrabi et al., 1996; Essa et al., 2014; Sigmund et al., 2014; Basha et al., 2016; Triller et al., 2024; Pallarés et al., 2021).

Table 2: Peak lateral strength and strength ratio for all specimens.

Reference	Frame Type	Loading	F_{max} (kN)	Strength Ratio
P.S.01	Bare frame	Monotonic	76.1	1.0 (reference)
P.S.02	Bare frame	Cyclic	76.4	1.0 (reference)
P.R.01	Infilled frame	Monotonic	196.7	2.6
P.R.02	Infilled frame	Cyclic	206.8	2.7

3.3 Ductility

Displacement ductility mu was evaluated using the definition of Crisafulli (1997) as the ratio of δ_2 to δ_1, where δ_1 and δ_2 are the lateral displacements at 85% of the peak resistance on the ascending and descending branches, respectively. Table 3 summarises the ductility results. Bare frames exhibited higher ductility (μ = 4.8 for P.S.01; μ = 5.6 for P.S.02) compared to infilled frames (μ = 4.3 for P.R.01; μ = 4.0 for P.R.02). This confirms that masonry infill, while dramatically increasing lateral strength and stiffness, reduces the inelastic deformation capacity of the system. A similar trend has been reported in the literature (Jiang et al., 2015; Essa et al., 2014).

Table 3: Ductility parameters for all specimens.

Reference	δ_1 (mm)	δ_{max} (mm)	δ_2 (mm)	δ_2/δ_{max}	μ
P.S.01	10.8	24.3	52.2	2.1	4.8
P.S.02	8.8	15.9	49.0	3.1	5.6
P.R.01	5.8	12.2	25.2	2.1	4.3
P.R.02	4.7	10.1	19.0	1.9	4.0

3.4 Initial Stiffness and Stiffness Degradation

Table 4 compares the initial lateral stiffness K_0 calculated from the initial linear portion of each force-displacement curve. Infilled frames exhibited initial stiffness values 5.3 times (P.R.01) and 4.4 times (P.R.02) higher than the corresponding bare frames. These enhancement factors are consistent with published ratios in the range 3-6 (Stylianidis, 2012; Pallarés et al., 2021).

Table 4: Initial lateral stiffness and stiffness ratio.

Reference	K_0 (kN/mm)	Stiffness Ratio
P.S.01	19.0	1.0 (reference)
P.S.02	25.2	1.0 (reference)
P.R.01	101.1	5.3
P.R.02	110.9	4.4

For cyclic specimens, the secant stiffness Ks of each load-unload cycle was determined from the line connecting the two extreme points of the cycle. Table 5 presents the cycle-by-cycle stiffness evolution. Both specimens exhibited continuous stiffness degradation with increasing displacement. The most severe stiffness loss occurred post-peak: P.R.02 lost 68% of its stiffness between cycles 3 and 4 (47.6 to 15.3 kN/mm), driven by extensive masonry crushing, while P.S.02 showed a comparatively moderate 31% reduction over the same interval.

Table 5: Stiffness degradation across load-unload cycles (kN/mm).

Reference	K_0	Cycle 1	Cycle 2	Cycle 3	Cycle 4	Cycle 5
P.S.02	25.2	16.1	11.3	8.3	6.4	5.7
P.R.02	110.9	97.8	81.4	47.6	15.3	-

3.5 Energy Dissipation

Energy dissipation in each load-unload cycle was calculated as the area enclosed by the hysteresis loop in the force-displacement diagram. Table 6 reports cycle-by-cycle and cumulative energy dissipation for P.S.02 and P.R.02 up to the load peak. The bare frame (P.S.02) dissipated marginally more cumulative energy than the infilled frame (P.R.02): 123.3 kN.mm versus 115.5 kN.mm, a difference of approximately 6.7%.

Table 6: Energy dissipation per cycle and cumulative (kN.mm).

Reference	Cycle 1	Cycle 2	Cycle 3	Cumulative
P.S.02	9.6	36.4	77.3	123.3
P.R.02	9.4	18.8	87.3	115.5

This result contrasts with findings from reversed-cycle (push-pull) experiments reported in the literature, where masonry-infilled frames typically dissipate 1.3 to 3.3 times more energy than bare frames (Zovkic et al., 2012; Essa et al., 2014; Jiang et al., 2015; Basha et al., 2016). The discrepancy is attributed to the push-over loading protocol used in the present study, which does not subject the specimen to reversed loading. Reversed cyclic loading activates additional damage mechanisms (repeated crack opening and closing, progressive mortar degradation) that significantly enhance energy dissipation in infilled frames.

3.6 Frame-Infill Interface Debonding Analysis

The DIC-based analysis of frame-infill interaction revealed that debonding between the masonry panel and the surrounding RC frame is the first irreversible phenomenon occurring in the infilled specimens. To quantify this, vertical and horizontal displacements were tracked at paired DIC points located on opposite sides of the frame-infill interface at three heights: upper, mid-height and lower. One point of each pair lay on the masonry wall surface (d_{yM}) and the other on the adjacent RC column surface (d_{yP}), initially separated by 8 cm.

Figure 7 presents vertical displacement profiles at all three levels for P.R.01 and P.R.02. At the upper and mid-height levels, the wall-side point exhibited consistently larger vertical displacement than the column-side point, indicating relative vertical slip (sliding) along the interface. At the lower level, displacements of the two sides remained nearly equal throughout, indicating that the lower portion of the interface remained substantially intact and that the panel acted monolithically with the frame in that region.

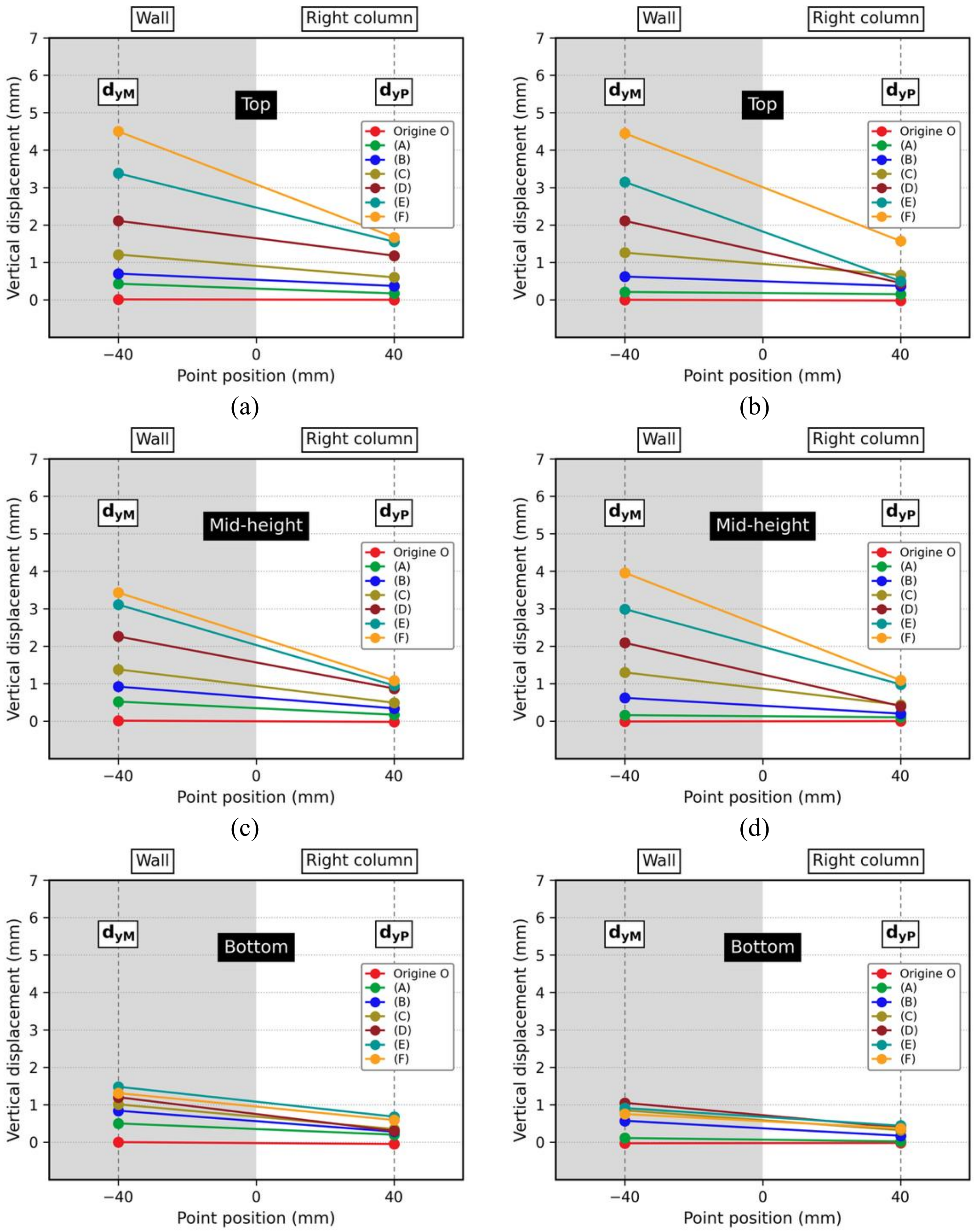

Figure 7. Vertical displacement profiles at upper, mid-height and lower levels, comparing wall-side (d_{yM}) and column-side (d_{yP}) points: (a, c, e) for P.R.01; (b, d, f) for P.R.02 (Source: Authors).

Significant interface slip developed from loading stage C onwards, corresponding to a lateral force of 147.9 kN (P.R.01) and 174.7 kN (P.R.02), approximately 75% of the respective peak resistance. These lateral displacements at stage C were approximately 4 mm and 5 mm respectively. The initiation of significant debonding coincides precisely with the formation of the fully developed diagonal crack pattern observed in the DIC strain maps. This suggests a physical coupling: once the diagonal compression strut is fully activated and the panel attempts to deform laterally while the frame resists, the limited mortar bond at the perimeter fails progressively, accelerating the relative sliding between panel and frame. This

sliding mechanism is consistent with the behaviour of masonry wallettes with soft or imperfect bed joints under static cyclic loading, where mortar joint quality has been shown to govern the onset and magnitude of relative slip along the interface (Vögeli et al., 2015).
The horizontal displacement field (Figure 8) confirmed this interpretation. At upper and mid-height levels, the frame column moved horizontally more than the masonry wall at the same height, particularly in the post-peak phase. This differential motion is consistent with localised crushing of the corner mortar and incomplete filling of the gap between the panel top edge and the beam soffit, conditions that arise from the construction sequencing typical in Algeria. Bikçe et al. (2021) systematically investigated RC frames with intentionally non-interacting (gap) infill walls and found that even small gaps significantly alter the load transfer mechanism and reduce the effective stiffness contribution of the infill, consistent with the debonding behavior observed in the present study.

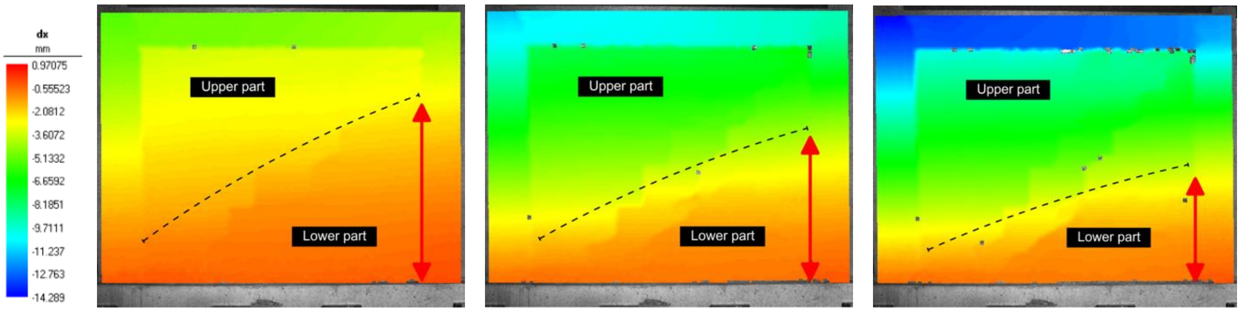

(a) (b) (c)

Figure 8. Horizontal displacement field at (a) pre-peak, (b) peak and (c) post-peak loading stages, from DIC analysis of P.R.01. The diagonal crack divides the panel into two zones with distinct displacement gradients (Source: Authors).

Principal strain direction maps obtained from DIC (Figure 9) revealed concentrated shear strains along the full frame-infill perimeter at the start of loading, with tensile stress concentrations developing at the upper-left corner and driving the initial panel separation. By peak load, the diagonal crack opened fully, and shear along the interface was reduced in the lower portion while remaining severe at the upper section. These observations confirm that the infill behaves monolithically with the frame only in its lower one-third, with the remainder of the perimeter subject to progressive debonding.

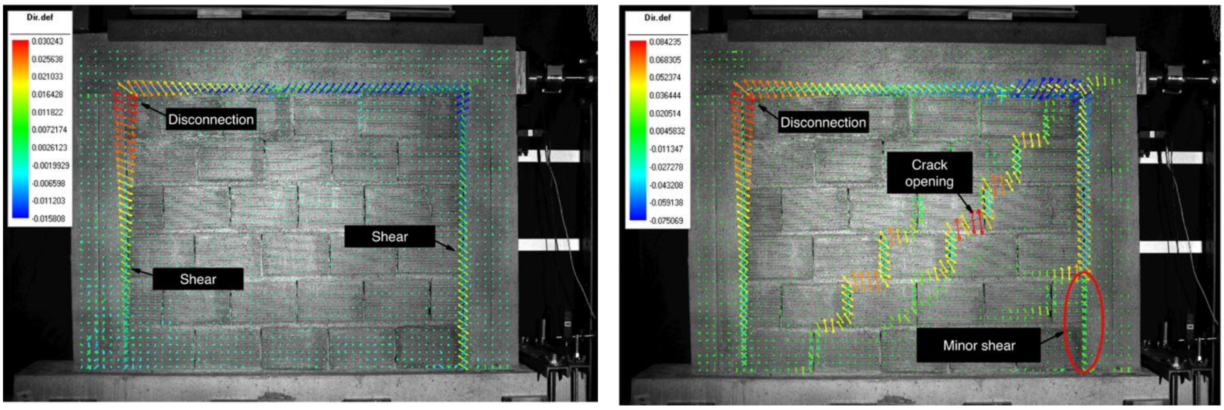

(a) (b)

Figure 9. DIC principal strain direction maps for P.R.02: (a) early-stage loading showing shear along perimeter and tensile disconnection at the upper-left corner; (b) at peak load showing fully opened diagonal crack and reduced lower-interface shear (Source: Authors).

4. Discussion

The experimental results collectively demonstrate that double-leaf masonry infill walls, constructed following current Algerian practice, significantly modify the seismic behaviour of RC frames in ways not captured by simplified code models that neglect infill contribution.
The strength enhancement factor of approximately 2.6-2.7 observed in the present study is consistent with a broad body of experimental literature and confirms the structural significance of masonry infill as a load-bearing element under seismic conditions. However, the simultaneous reduction in ductility by approximately 10-15% compared to bare frames underscores the trade-off inherent in infilled systems: gains in lateral strength come at the cost of reduced inelastic deformation capacity. In design practice, this means that structures relying on post-yield ductility for seismic energy absorption may be less effective when masonry infills are present unless the infill distribution and frame detailing are carefully co-ordinated.
The stiffness enhancement factors of 4.4-5.3 reported here are at the upper end of values documented in the literature (Stylianidis, 2012) and are attributable to the double-leaf construction and to the relatively tight fit of the infill within the frame bays. Stiffness degradation during cyclic loading was much more severe for the infilled frame (P.R.02), where 68% of the secant stiffness was lost between cycles 3 and 4, driven by the sudden and extensive crushing of masonry at the

loaded corners. This sharp degradation has important implications for the assessment of cumulative damage during an earthquake, where many cycles at various amplitudes must be sustained.

The DIC analysis provided previously unattainable detail on the debonding mechanism at the frame-infill interface. The finding that significant interface slip begins at approximately 75% of peak resistance, and coincides with full diagonal strut formation, has direct implications for structural modelling. Equivalent strut macro-models, which assume full bond between the panel and the frame throughout loading, overestimate the stiffness contribution of the infill at large drifts and mis-represent the load path to the beam-column joints. A more accurate representation would incorporate a contact-friction interface element that captures the progressive debonding identified here (Dhir et al., 2021; Dhir et al., 2022). Sreekeshava et al. (2023) demonstrated that interface strengthening with geo-fabric can significantly improve frame-infill interaction and load transfer, further confirming that interface behavior is a critical and controllable parameter in the seismic performance of infilled frames.

The construction sequence effect observed in the present study - where building the infill wall after the frame produces an imperfect perimeter joint that triggers early and extensive debonding - contrasts sharply with the behaviour of confined masonry, in which the RC columns are cast after the masonry wall and the two systems are effectively bonded from the outset. In confined masonry, Ghorbani et al. (2014) found that interface slip remained negligible throughout loading, with the panel acting monolithically with the frame and contributing to lateral resistance from the earliest loading stages. The contrast underscores a critical construction-practice dependency: seismic performance assessments of RC frames with masonry infills must account for the as-built interface condition rather than relying on idealised bond assumptions. Del Vecchio et al. (2022) reached similar conclusions from full-scale pseudo-dynamic tests on two-storey RC frames with different infill-to-structure connections, demonstrating that connection detailing and construction sequence have first-order effects on seismic response and damage distribution.

The energy dissipation results require careful interpretation. The marginal superiority of the bare frame (P.S.02) over the infilled frame (P.R.02) in cumulative energy dissipation under push-over cyclic loading is inconsistent with the broader literature on reversed-cycle loading. The push-over protocol does not activate the crack re-closure and friction mechanisms that are central to the hysteretic energy dissipation of masonry-infilled frames under real seismic reversed cycling. Future experiments on similar specimens under fully reversed cyclic loading are needed to characterise energy dissipation more completely and to evaluate fatigue-related damage accumulation.

5. Conclusions

This study set out to characterise the in-plane lateral behaviour of half-scale RC frames with and without double-leaf masonry infill walls, to identify their failure modes, and, using full-field Digital Image Correlation (DIC), to quantify the frame–infill interface debonding that results from the prevailing Algerian construction sequence. The four research objectives were met, and the main findings are summarised as follows:

- Masonry infill increased peak lateral strength by 2.6-2.7 times and initial stiffness by 4.4-5.3 times relative to bare frames, confirming that infills act as primary lateral-load-resisting elements rather than non-structural partitions. This gain came at the cost of reduced displacement ductility (μ = 4.0-4.3 for infilled frames versus 4.8-5.6 for bare frames) and far more severe cyclic stiffness degradation (a 68 % post-peak loss for the infilled frame against 31 % for the bare frame). Bare frames failed by flexural hinging at the beam-column joints, whereas infilled frames developed the classical diagonal-strut mechanism with staircase cracking and corner crushing. DIC revealed that interface debonding initiates at the upper panel corner at a very early load stage, propagates around the perimeter, and becomes significant at approximately 75 % of peak resistance, coinciding with full diagonal-strut formation, while only the lower one-third of the interface remained monolithically bonded.
- These results directly confirm the study's central premise: that the construction sequence, building the infill after the frame, produces an imperfect perimeter joint that governs the onset and propagation of debonding, and thereby shapes the entire seismic load path. The full-field measurements provided the quantitative evidence needed to establish this link, which point-wise instrumentation could not have resolved.
- The study contributes to the existing body of knowledge in two ways. Methodologically, it validates DIC as an advanced, quantitative diagnostic tool for mapping complex frame-wall interactions and interface kinematics. Substantively, it provides experimental evidence that widely used equivalent diagonal-strut models, which assume a full frame-infill bond throughout loading, overestimate the infill contribution at large drifts and misrepresent the shear demand transferred to the beam–column joints; a contact-friction interface formulation is therefore recommended for as-built, non-integral infills typical of North-African and similar construction practice.
- The cyclic protocol used here was of the load–unload (push-over) type and did not capture the fatigue and crack re-closure mechanisms mobilised under fully reversed loading; this explains the marginally lower cumulative energy dissipation measured for the infilled frame. Future research should therefore employ fully reversed cyclic loading, extend the programme to multi-bay and multi-storey configurations, and use the present DIC dataset to calibrate and validate numerical contact-friction interface models.

Acknowledgements

The authors gratefully acknowledge the technical and scientific support provided by the LOCIE Laboratory at the Universite Savoie Mont Blanc (France) and the LGCA Laboratory at Universite Echahid Cheikh Larbi Tebessi (Algeria). The authors thank the laboratory technical staff for their assistance during specimen construction and testing.

Funding
This research was supported by the Algerian Ministry of Higher Education and Scientific Research, the Applied Civil Engineering Laboratory (LGCA) of Echahid Cheikh Larbi Tebessi University, Tebessa, Algeria, and the LOCIE Laboratory of Universite Savoie Mont Blanc, Chambery, France. The authors gratefully acknowledge the financial and material resources provided by these institutions throughout the experimental program.

Conflicts of Interest
The author(s) report no conflicts of interest.

Data Availability Statement
The data presented in this study are available on reasonable request from the corresponding author.

Institutional Review Board Statement
Not applicable. This study did not involve human participants, animals, or clinical trials.

CRediT Author Statement
Layadi Ismail: Conceptualisation; Methodology; Investigation; Formal Analysis; Writing - original draft; Writing - review and editing. All authors have read and approved the final manuscript.

References
Basha, S. H., & Kaushik, H. B. (2016). Behavior and failure mechanisms of masonry-infilled RC frames (in low-rise buildings) subject to lateral loading. Engineering Structures, 111, 233–245. https://doi.org/10.1016/j.engstruct.2015.12.034

Bhat, Z. M., Singh, Y., & Agarwal, P. (2024). Cyclic testing and diagonal strut modelling of different types of masonry infills in reinforced concrete frames designed for modern codes. Engineering Structures, 317, 118695. https://doi.org/10.1016/j.engstruct.2024.118695

Bikçe, M., Emsen, E., Erdem, R. T., & Bayrak, T. (2021). An investigation on behavior of RC frames with non-interacting infill wall. Engineering Structures, 245, 112920. https://doi.org/10.1016/j.engstruct.2021.112920

Crisafulli, F. J. (1997). Seismic behaviour of reinforced concrete structures with masonry infills [Doctoral dissertation, University of Canterbury]. Department of Civil Engineering, University of Canterbury, Christchurch, New Zealand. https://doi.org/10.26021/1979

Del Vecchio, C., Di Ludovico, M., Verderame, G. M., & Prota, A. (2022). Pseudo-dynamic tests on full-scale two storeys RC frames with different infill-to-structure connections. Engineering Structures, 266, 114608. https://doi.org/10.1016/j.engstruct.2022.114608

Demirel, İ. O., Binici, B., & Yakut, A. (2023). In-plane seismic performance of different infill wall systems in ductile reinforced concrete frames. Bulletin of Earthquake Engineering, 21(7), 3433–3459. https://doi.org/10.1007/s10518-023-01663-5

Dhir, P. K., Tubaldi, E., Ahmadi, H., & Gough, J. (2021). Numerical modelling of reinforced concrete frames with masonry infills and rubber joints. Engineering Structures, 246, 112833. https://doi.org/10.1016/j.engstruct.2021.112833

Dhir, P. K., Tubaldi, E., Pantò, B., & Caliò, I. (2022). A macro-model for describing the in-plane seismic response of masonry-infilled frames with sliding/flexible joints. Earthquake Engineering & Structural Dynamics, 51(12), 3022–3044. https://doi.org/10.1002/eqe.3714

Essa, A. S. A., Badr, M. R. K., & El-Zanaty, A. H. (2014). Effect of infill wall on the ductility and behavior of high strength reinforced concrete frames. HBRC Journal, 10(3), 258–264. https://doi.org/10.1016/j.hbrcj.2013.12.003

Ghorbani, M., Alam, M. S., & Kobraei, M. (2014). An experimental study on the seismic behavior of confined masonry walls. KSCE Journal of Civil Engineering, 18(7), 2176–2188. https://doi.org/10.1007/s12205-014-0503-0

Grubišić, M., Kalman Šipoš, T., Grubišić, A., & Pervan, N. (2023). Testing of damaged single-bay reinforced concrete frames strengthened with masonry infill walls. Buildings, 13(4), 1021. https://doi.org/10.3390/buildings13041021

Jiang, H., Liu, X., & Mao, J. (2015). Full-scale experimental study on masonry infilled RC moment-resisting frames under cyclic lateral loading. Engineering Structures, 91, 70–84. https://doi.org/10.1016/j.engstruct.2015.02.008

Kallioras, S., Pohoryles, D. A., Bournas, D., Molina, F. J., & Pegon, P. (2023). Seismic performance of a full-scale five-story masonry-infilled RC building subjected to substructured pseudodynamic tests. Earthquake Engineering & Structural Dynamics, 52(12), 3649–3678. https://doi.org/10.1002/eqe.3940

Lu, Y ., Lv, J., & Liu, Y . (2024). Hysteresis performance and damage mode of self-centering frame with masonry infill wall: Experimental study assisted with DIC technique. Engineering Structures, 318, 118797. https://doi.org/10.1016/j.engstruct.2024.118797

Mehrabi, A. B., Shing, P. B., Schuller, M. P., & Noland, J. L. (1996). Experimental evaluation of masonry-infilled RC frames. Journal of Structural Engineering, 122(3), 228–237. https://doi.org/10.1061/(ASCE)0733-9445(1996)122:3(228)

Pallarés, F. J., Davia, A., Hassan, S. A. S., & Pallarés, L. (2021). Experimental and analytical assessment of the influence of masonry façade infills on seismic behavior of RC frame buildings. Engineering Structures, 235, 112031. https://doi.org/10.1016/j.engstruct.2021.112031

Pokharel, T., Biswal, A., Sahoo, D. R., & Dhir, P. K. (2024). Seismic performance of masonry-infilled RC frames and its implications in design approach: A review. Practice Periodical on Structural Design and Construction, 29(2), 04024006. https://doi.org/10.1061/ppscfx.sceng-1337

Sciuti, V. F., Vargas, R., Guerrero, N., Marante, M. E., & Hild, F. (2025). Digital image correlation analyses of masonry infilled frame: Uncertainty-based mesh refinement and damage quantification. Mathematics and Mechanics of Solids, 30(2), 364–388. https://doi.org/10.1177/10812865231174840

Sigmund, V., & Penava, D. (2014). Influence of openings, with and without confinement, on cyclic response of infilled R-C frames — An experimental study. Journal of Earthquake Engineering, 18(1), 113–146. https://doi.org/10.1080/13632469.2013.817362

Sreekeshava, K. S., Rodrigues, H., & Arunkumar, G. (2023). Response of masonry-infilled reinforced concrete frames strengthened at interfaces with geo-fabric under in-plane loads. Buildings, 13(6), 1495. https://doi.org/10.3390/buildings13061495

Stylianidis, K. C. (2012). Experimental investigation of masonry infilled R/C frames. The Open Construction and Building Technology Journal, 6(1), 194–212. https://doi.org/10.2174/1874836801206010194

Triller, P., Kwiecień, K., Kwiecień, A., Bohinc, U., Zając, B., & Tekieli, M. (2024). Efficiency of FRPU strengthening of a damaged masonry infill wall under in-plane cyclic shear loading and elevated temperatures. Engineering Structures, 317, 118652. https://doi.org/10.1016/j.engstruct.2024.118652

Vacher, P., Dumoulin, S., Morestin, F., & Mguil-Touchal, S. (1999). Bidimensional strain measurement using digital images. Proceedings of the Institution of Mechanical Engineers, Part C: Journal of Mechanical Engineering Science, 213(8), 811–817. https://doi.org/10.1243/0954406991522428

Vögeli, C., Mojsilović, N., & Stojadinović, B. (2015). Masonry wallettes with a soft layer bed joint: Behaviour under static-cyclic loading. *Engineering Structures*, *86*, 16–32. https://doi.org/10.1016/j.engstruct.2014.12.038

Zovkic, J., Sigmund, V., & Guljaš, I. (2013). Cyclic testing of a single bay reinforced concrete frames with various types of masonry infill. Earthquake Engineering & Structural Dynamics, 42(8), 1131–1149. https://doi.org/10.1002/eqe.2263